Production and Depletion of Supercooled Liquid Water in a Colorado Winter Storm

MARCIA K. POLITOVICH AND BEN C. BERNSTEIN

Research Applications Program, National Center for Atmospheric Research, Boulder, Colorado.

(Manuscript received 2 December 1994, in final form 15 June 1995)

ABSTRACT

During the 1990 Winter Icing and Storms Project (WISP), a shallow cold front passed through northeastern Colorado, followed by a secondary cold front. A broad high pressure area behind the initial front set up a Denver cyclone circulation within a well-mixed boundary layer, which was capped by a stable, nearly saturated layer of air left in place by the initial cold front. As the secondary cold front passed through the WISP domain, these layers of air were lifted. The lifted boundary layer formed only broken cloud, but the lifted moist layer formed a stratiform cloud that contained high liquid water contents. Cloud characteristics were measured in situ with a research aircraft, and remotely by ground-based radars, microwave radiometers, and a lidar ceilometer. Moderate to severe icing conditions were reported by aircraft flying in the area during the event and also affected the flight of the research aircraft through an increase in drag on the airframe. Liquid water was depleted in portions of the lower stratiform cloud as ice crystals, produced in midlevel clouds embedded in westerly flow, fell into the lower cloud, and quickly rimed to form showers of graupel at the ground. After these midlevel clouds passed over the area, liquid production resumed. Supercooled liquid cloud persisted for 36 h as cloud formed within the surface cold air mass behind the secondary cold front as it entered the Denver area and was lifted over the local terrain.

The evolution of weather events is discussed using a variety of datasets, including radar, surface mesonet, balloon-borne soundings, research aircraft, satellite imagery, microwave radiometers, and standard National Weather Service observations. By combining information from these varied sources, processes governing the production and depletion of supercooled liquid from the synoptic to the microscale are examined. The storm is also discussed in terms of its potential for causing moderate to severe aircraft icing. The effect of accreted ice on the research aircraft is described, as are implications of the meteorology for detection and forecasting in-flight icing.

1. Introduction

On 27 February 1990, during the Winter Icing and Storms Project (WISP), a cold front passed through the Colorado Front Range area, followed 24 h later by a strong secondary front, which produced a widespread upslope cloud composed primarily of supercooled liquid water droplets. Infrared satellite imagery indicated that the cloud extended from the Rocky Mountains to the eastern Colorado border. Aircraft in the Denver area reported moderate to severe icing conditions. At 0248 UTC 28 February, a Cessna 208 crashed on approach to Stapleton International Airport, killing the pilot. While evidence is inconclusive, icing of the airframe is suspected as a cause or factor in the accident.

The goals of WISP are twofold: to understand the production and depletion of supercooled liquid water in winter storms, and to improve forecasts of in-flight aircraft icing (Rasmussen et al. 1992). This storm provides an opportunity to address both goals. It has long been understood that lifting of air, with subsequent cooling, produces liquid water in clouds. Also, "seeder–feeder" mechanisms, by which ice falling into a supercooled liquid cloud from above depletes liquid, have been documented previously as discussed by Reinking and Boatman (1987). The characteristics of aircraft icing environments have been examined from a climatological aspect (Cooper et al. 1984; Jeck 1983; Cober et al. 1995) and from case studies with some meteorological data but concentrated on their effects on flight (as in Sand et al. 1984; Politovich 1989). This paper will combine a unique set of measurements, from synoptic to microscale, to describe those processes governing the formation of the icing environment, as well as the nature of that icing environment through pilot reports of icing and its effect on the flight characteristics of a research airplane encountering that environment.

Measurements obtained during the event to document the processes involved in supercooled liquid water production and depletion will be presented, including those associated with the passage of a secondary cold front. The structure of a Denver cyclone circulation and its interaction with the secondary front are discussed. Microphysical processes associated with liquid depletion, as revealed by aircraft, radar, and radiometer measurements, are described in detail. The effect of

Corresponding author address: Dr. Marcia K. Politovich, National Center for Atmospheric Research, P.O. Box 3000, Boulder, CO 80307.

accreted ice on the flight of the research aircraft is discussed, as are implications of this case for forecasting in-flight icing.

2. Data sources

The 1990 WISP field project (WISP90) was conducted along the Front Range of the Colorado Rocky Mountains from 1 February to 31 March. Extensive remote and in situ measurement facilities were available, including a surface mesonet, three microwave radiometers, four balloon-sounding sites, two Doppler radars, and a research aircraft (see Fig. 1). Measurements from these instruments and standard National Weather Service (NWS) observations will be incorporated into the discussion.

a. Surface and upper-air measurements

The WISP90 surface measurement network consisted of 19 National Center for Atmospheric Research (NCAR) Portable Automated Mesonet (PAM) and 22 National Oceanic and Atmospheric Administration (NOAA) Forecast Systems Laboratory (FSL) stations. The stations recorded 5-min averages of temperature, dewpoint, wind speed and direction, pressure, accumulated precipitation, and global solar radiation (FSL only). FSL dewpoint measurements were made using a cooled mirror, while all PAM stations used a psychrometer. Some of the PAM stations were also equipped with Rotronics humidity sensors to obtain higher quality dewpoint measurements at temperatures below freezing. Additional surface measurements were also provided by the NWS surface airways observation (SAO) sites in the WISP area.

Four NCAR Cross-chain Loran Atmospheric Sounding System (CLASS) sites were operated during WISP90 to obtain measurements of the vertical structure of temperature, dewpoint, and winds. These sites were collocated with PAM or SAO sites to obtain quality surface data. CLASS launches were usually made at 3-h intervals during intensive operation periods. The data were recorded at 10-s intervals, which roughly corresponds to 50-m vertical resolution. Additional sounding data were provided by NWS balloon launches twice daily at Denver (DEN).

b. Remote sensors

Two Doppler radars were operated in the Denver area during WISP90. The Mile High Radar (MHR) was located about 15 km northeast of Denver. This radar has a wavelength of 10 cm, a 0.9° half-power beamwidth, and 225-m gate spacing. The NCAR CP-3 radar was located at Marshall, about 38 km west-northwest of the MHR, and has a 5-cm wavelength, a

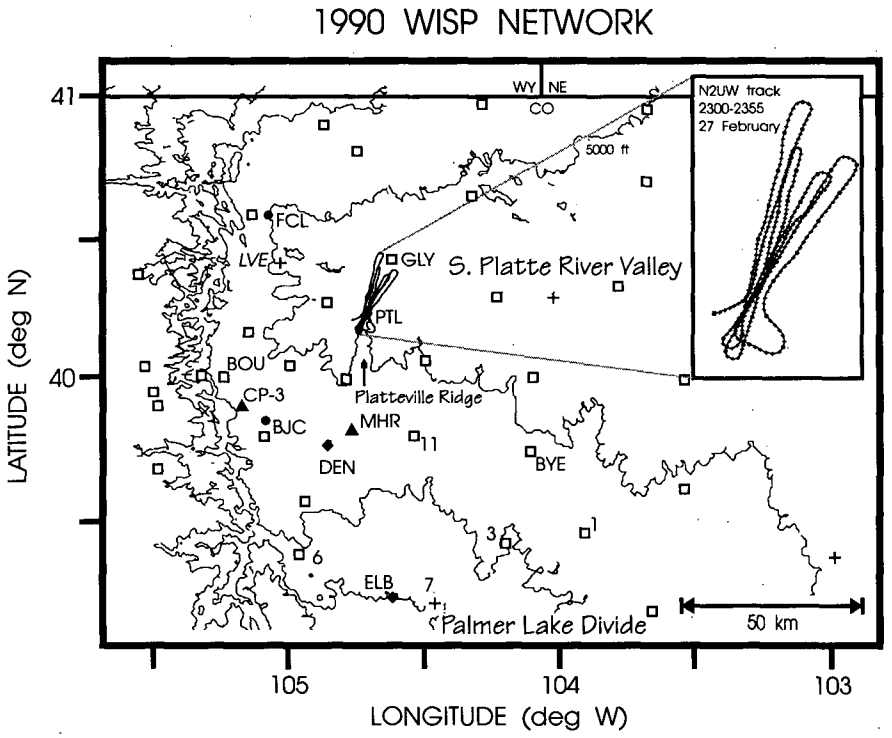

FIG. 1. Map of the WISP90 network. Locations of mesonet stations (□), radars (▲), radiometers (♦), CLASS soundings (+), and NWS surface observations (●), contours of elevation every 1000 ft (330 m), and approximate position of *N2UW* flight tracks are shown.

0.9° half-power beamwidth, and 150-m gate spacing. The NOAA Environmental Technology Laboratory operated three dual-channel (20.6 and 31.65 GHz) microwave radiometers during WISP90 at Platteville, Denver, and Elbert (PTL, DEN, and ELB on Fig. 1). The radiometers provided measurements of total integrated liquid water and water vapor at 2-min intervals for columns directly above the sites. Retrieval of these quantities from measurements of the two brightness temperatures is as described by Hogg et al. (1983), and spurious measurements were removed in postanalysis by applying quality control algorithms as described by Stankov et al. (1990). Theoretical predictions, valid for nonprecipitating clouds, indicate that the radiometer can measure integrated liquid with approximately 10% accuracy (Westwater 1993). Hill (1992) presented a comparison of aircraft- and radiometer-based integrated liquid measurements that showed good agreement between the values and a correlation coefficient of 0.94.

c. *Research aircraft*

The University of Wyoming King Air research aircraft was used to provide in situ measurements of cloud structure. This aircraft was fully equipped for cloud physics and atmospheric state parameter measurements and was certified for flight into known icing conditions. Instrumentation is described fully by Cooper et al. (1984). For this study, 1-s values of standard meteorological variables were used, including temperature, dewpoint, and pressure, aviation variables such as airspeed and rate of climb, and microphysical variables such as cloud liquid water, droplet size spectrum, and two-dimensional images of cloud particles. Liquid water measurements in this paper are from a King liquid water detector (King et al. 1978). Cloud droplet size distributions were measured using a Particle Measuring System (PMS) forward-scattering spectrometer probe (FSSP) that was operated on the 2–30-μm range. Airspeed corrections as described by Cerni (1982) were applied to the data. A PMS 1D-C probe was used for measurements of hydrometeor concentration and maximum dimension in the 12.5–187.5-μm diameter range. Images of hydrometeors were collected using PMS 2D-C and 2D-P probes, which measure diameters from 25 to 800 and 200 to 6400 μm, respectively. All particle types were determined by visual inspection of 2D-C images. In addition to the datasets from *N2UW*, pilot reports from general aviation and commercial aircraft were used to determine the times and the locations of icing.

d. *Volunteer snow observers*

A network of approximately 100 volunteer weather observers was in place for WISP90. These volunteers were recruited to take measurements of snowfall, liquid equivalent, crystal type and size, aggregation, and degree of riming. Time resolution and quality of these data varied by observer. The network was most dense near Boulder, Fort Collins, and Denver, but sparse observations were available from more remote locations within the WISP90 domain. Details of the volunteer snow observer network are described by Bernstein et al. (1992).

3. Synoptic and mesoscale structure

a. *Synoptic overview*

At 1800 UTC[1] 26 February 1990, a cold front associated with a broad high pressure system centered in southwestern Canada moved southward toward the Colorado–Wyoming border. Figure 2 shows the progression of this front through the central United States, along with the 500-mb geopotential height pattern at 1200 27 February. By 0000 27 February, the cold front had moved southward through northeastern Colorado (Fig. 2b). Behind the front, surface winds shifted to northeasterly and some midlevel clouds formed, but no precipitation was observed. During 27 February, the high pressure center in Canada became elongated and extended southeastward to the northern Montana border. As the high pressure center strengthened to 1040 mb and moved into western North Dakota, the pressure gradient over the WISP domain changed to one favoring easterly, and finally, southeasterly geostrophic winds (Figs. 2c and 3a). This led to the formation of a cyclonic circulation known as the Denver cyclone (Szoke 1991), which was fully developed by 1500 27 February. These circulations have been shown to form in the Denver vicinity due to the interaction of southerly and southeasterly flow having low Froude number with the Palmer Lake Divide and Front Range of the Colorado Rockies (Wilczak and Christian 1990; Crook et al. 1990).

The 500-mb geopotential height pattern suggests light confluent winds over Colorado (see Fig. 2d). A weak low was located over the California–Arizona border, with an attendant short wave, causing minor geopotential height falls in southwest Colorado. By 2100, a secondary surface cold front moved southward to the Colorado–Wyoming border. This front was not sharply defined as it passed through Casper and Cheyenne, Wyoming, as only light snow and a shift to northeasterly winds were recorded with its passage. The front became more obvious as it passed through northeastern Colorado between 2100 and 0300 28 February.

b. *Formation of a Denver cyclone circulation*

As the surface high pressure center progressed southeastward from Montana, early on 27 February,

[1] All times are UTC.

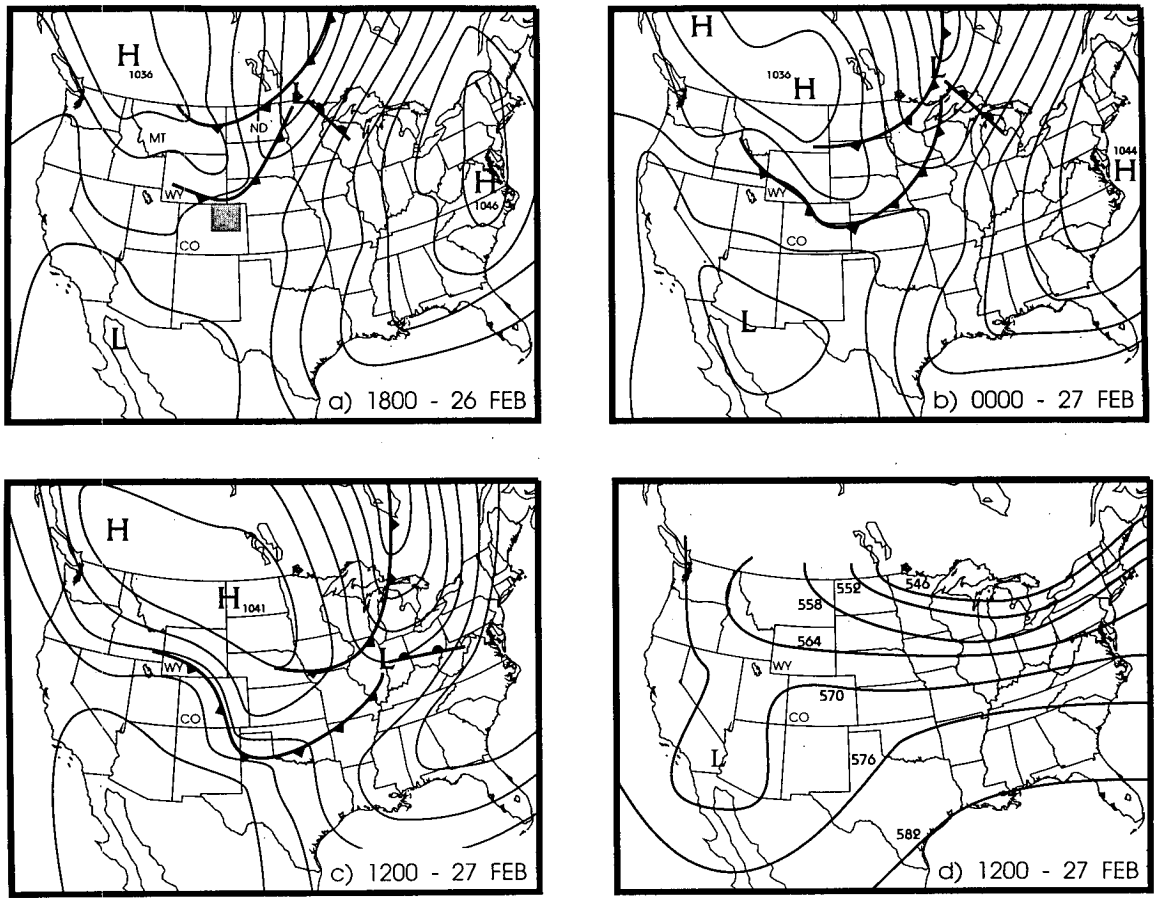

FIG. 2. Surface maps for (a) 1800 UTC 26 February, (b) 0000 UTC 27 February, and (c) 1200 UTC 27 February, along with (d) 500-mb map for 1200 UTC 27 February. Solid lines on (a)–(c) are isobars every 4 mb, solid lines on (d) are geopotential heights every 60 m. A shaded box in (a) denotes the extent of the WISP network from Fig. 1.

the surface pressure gradient over eastern Colorado became oriented from southwest to northeast. By 0900 27 February southeasterly and easterly winds of 5 m s^{-1} existed across the mesonet, except for weak northerly winds that began to form along the foothills of the Rocky Mountains (not shown). By 1500 (see Fig. 3a), a Denver cyclone circulation formed and became quite distinct, with northerly flow along the foothills of the Rocky Mountains from Fort Collins (FOR) to Sedalia (PAM-6). A north–south convergence line, with values eventually exceeding 2×10^{-4} s^{-1} at 2100, divided the northerly winds to the west from southerly winds to the east. At 1500, this axis (dashed line in Fig. 3a) extended from just south of Greeley (GLY) between DEN and PAM-11 to between PAM-6 and Elbert (ELB). Over the next 6 h, the circulation intensified while its axis bowed toward the east (Fig. 3b).

Analysis of surface-measured equivalent potential temperature θ_e at 2100 (Fig. 3b) reveals distinctly different air masses on either side of the axis with values to the east as much as 4 K higher than those to the west. Wilczak and Christian (1990) noted a similar structure in θ_e in their case study of a Denver cyclone, explaining that plumes of higher θ_e to the east were advected off of the higher terrain of the Palmer Divide, while lower values to the west were the result of the southward advection of cool air from the Platte Valley.

c. *Evolution of the vertical structure, 1500–2100 UTC 27 February*

The 1500 Loveland (LVE) sounding was obtained within the northwest quadrant of the Denver cyclone and shows several distinct layers (see Figs. 4a and 5). Closest to the ground, a 500-m-deep, slightly stable boundary layer with light northeasterly winds existed, which contained the Denver cyclone circulation. Above this, the air was nearly saturated and isothermal for another 500 m, and represents the initial cold front. Broken clouds were reported within this layer at the nearby Fort Collins SAO site (FCL). A thin transition layer, 470 m in depth, separated the cold frontal air from the westerlies aloft, with a temperature inversion of nearly 5°C. Finally, a moist layer was present from

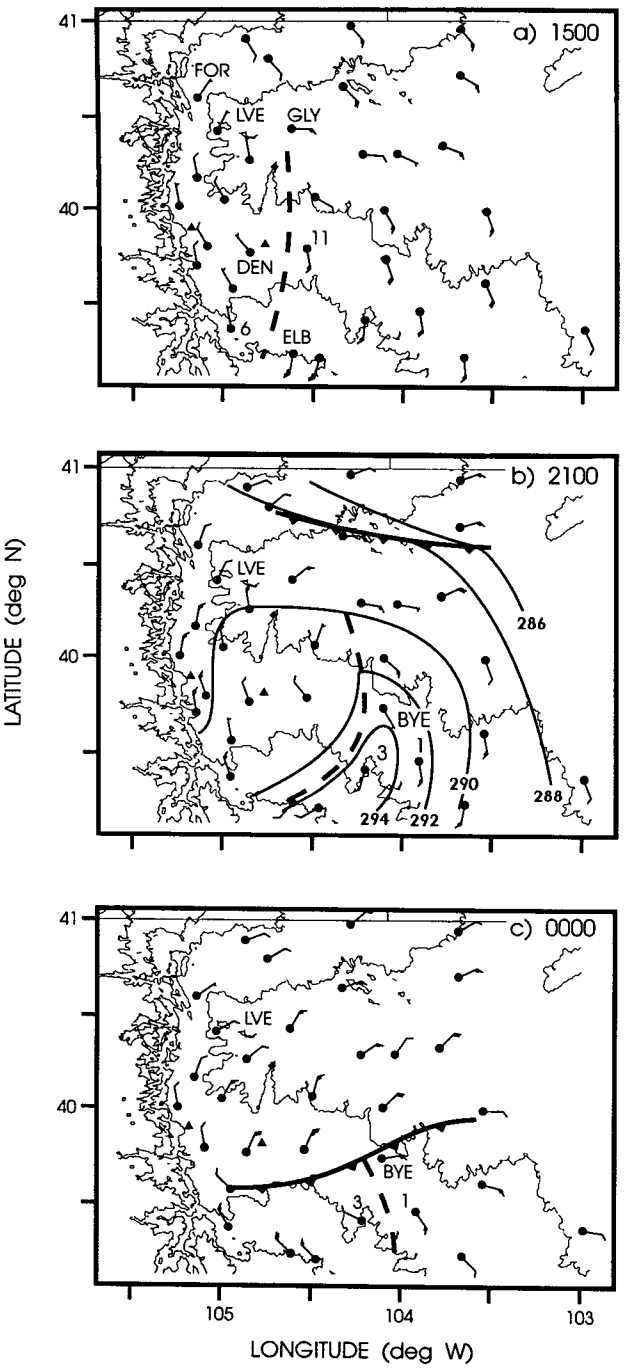

FIG. 3. Surface mesonet winds at 1500 and 2100 UTC 27 February and 0000 UTC 28 February. A full wind barb is 5 m s^{-1}, a half barb is 2.5 m s^{-1}. Positions of the secondary cold front (solid, barbed lines) and the Denver cyclone axis (heavy, dashed line) are shown; contours of surface θ_e (solid, thin lines) every 2 K are shown at 2100 UTC.

about 4 km to the tropopause. This highest layer of air was saturated with respect to ice above 6 km. From infrared satellite data (not shown) and the 1500 LVE sounding, an isolated area of cloud from approximately 6 to 10 km, with a top temperature of about −50°C, is indicated. This cloud was limited to the northwestern portion of the WISP domain and appears to have been induced by deep wave activity over the Rocky Mountains.

A time–height cross section of sounding data from Loveland (Fig. 5) shows that the well-mixed boundary layer deepened to 2.5 km MSL by 2100 27 February with θ becoming nearly constant with height. Winds within the layer strengthened to 10 m s^{-1} and developed a stronger upslope component between 1800 and 2100. As the low-level upslope flow and boundary layer developed, they lifted the moist air above by about 500 m. Figure 5 shows this lifting as a gradual sloping of the θ contours; θ_e behavior was similar. Lifting the 1800 Loveland sounding produces a structure nearly identical to that observed in the 2100 sounding. During this time, light snow fell from the cold cloud in the moist layer aloft, moistening and slightly cooling the atmosphere down to 3.9 km at 1800. The original cold-frontal inversion was substantially weakened by 2100 due to this cooling of the air above it (see Figs. 4a and 5). Some of the snow crystals appear to have survived to reach the surface as a narrow area of 5–10-dBZ reflectivity was present near Loveland between 1730 and 1900 (not shown). The snow ended just after 1900 as the wave-induced upper cloud deck dissipated, leaving the layer of westerly flow aloft moist but unsaturated.

d. Arrival of the secondary cold front

At around 2100 27 February, a secondary cold front entered northeastern Colorado, as shown in Fig. 3b. The front was first detected as a shift in wind direction to northeast at mesonet stations just south of the Wyoming border. Changes in temperature, pressure, and wind speed were gradual at these sites. As the front entered the South Platte River valley between 2100 and 2200 27 February, it encountered a discontinuity in winds over a relatively small distance, with southerly winds on the east side of the Denver cyclone axis, and northerly winds on the west side. Southward progress of the front became slower on the east side, at 3.9 m s^{-1}, than on the west, at 9.9 m s^{-1}. The wind discontinuity also altered the character of frontal passage on either side of the cyclone axis. A comparison of frontal passage at two stations on opposite sides of the axis is shown in Fig. 6. Station PAM-3, on the west side of the axis, had prefrontal northwesterly winds at 2.5 m s^{-1}, along with steady temperatures of approximately 1.5°C, at 0100 28 February. Note the passage of the Denver cyclone axis at 2130, 27 February, which was accompanied by a sudden wind shift and 2°C drop in temperature. Frontal passage at this station was quite obvious at 0130 when the winds increased to 9 m s^{-1}, the wind direction shifted, and the temperature dropped 3°C in 10 min. Strong easterly winds, falling temperature, and rising pressure continued at that site

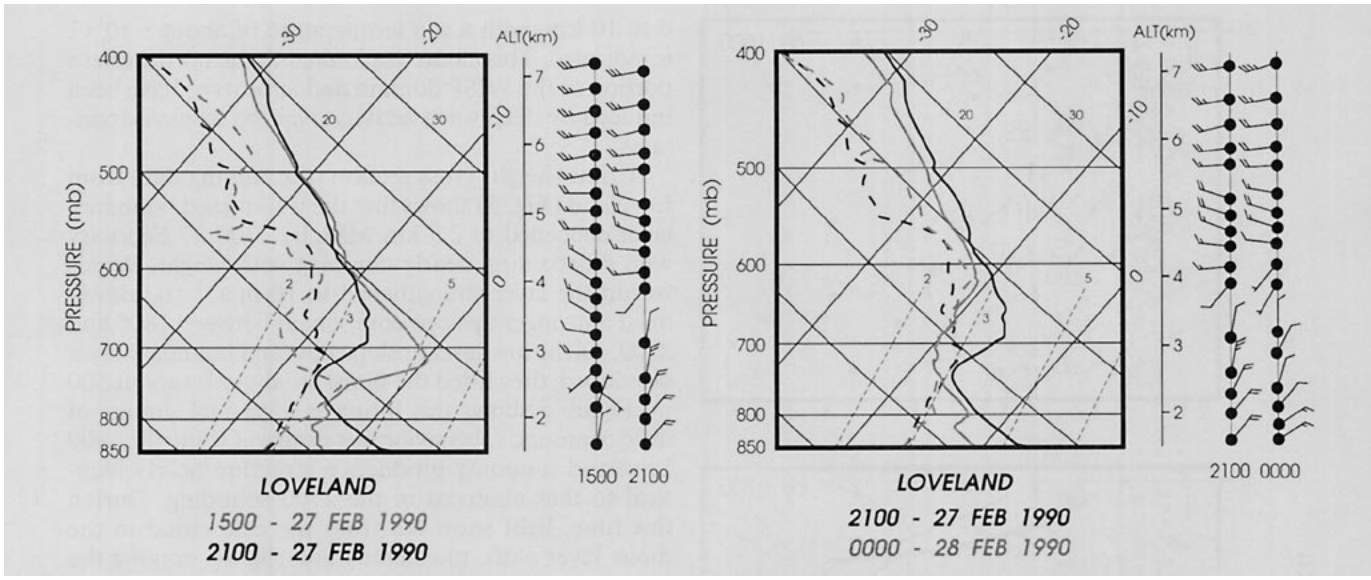

FIG. 4. CLASS data from Loveland. (a) Sounding of temperature T, dewpoint T_D, and wind barbs for 1500 and 2100 UTC 27 February. (b) Same as (a) but for 2100 UTC 27 February and 0000 UTC 28 February.

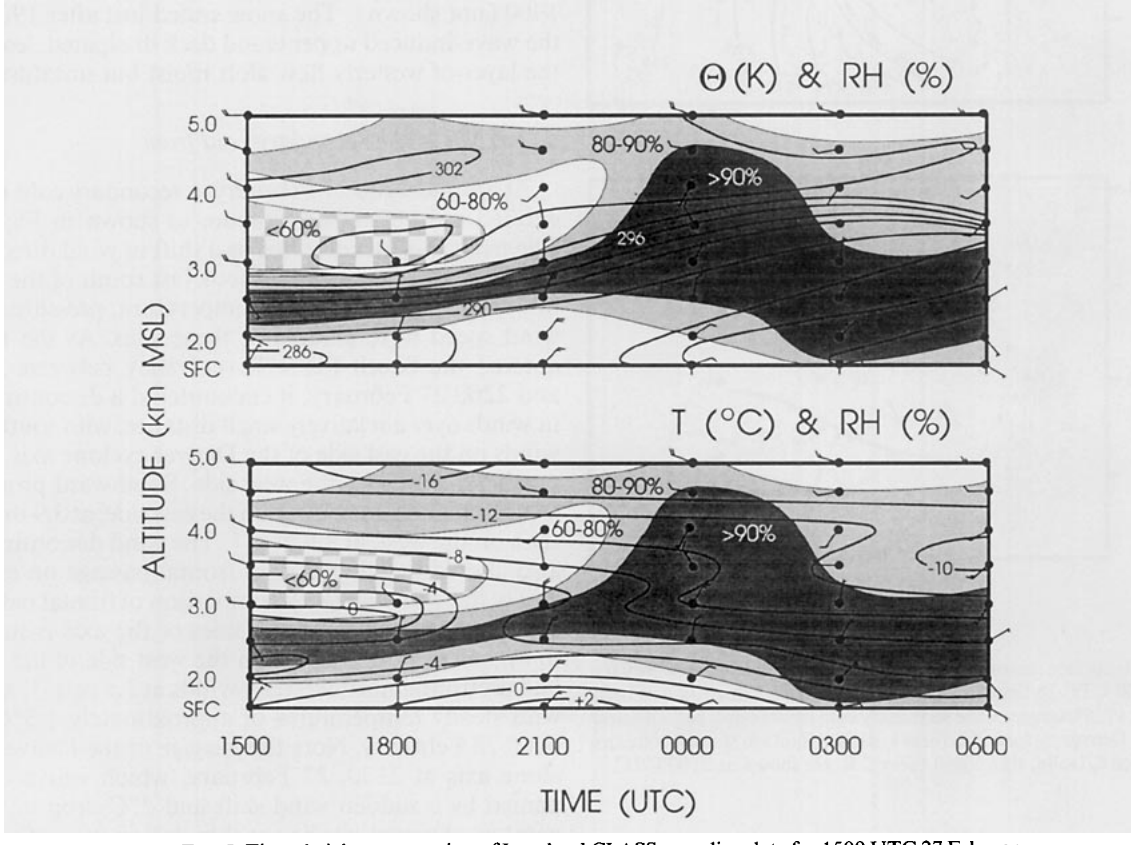

FIG. 5. Time–height cross section of Loveland CLASS sounding data for 1500 UTC 27 February to 0600 UTC 28 February. The top diagram shows θ (K) as solid lines and relative humidity RH of less than 60%, 60%–80%, 80%–90%, and greater than 90% as hatched, white, light gray, and dark gray shaded areas, respectively. Contours of θ are every 2 K. The bottom diagram shows temperature (°C) with RH overlain. Contours of T are every 2°C. Full wind barbs are 5 m s^{-1}.

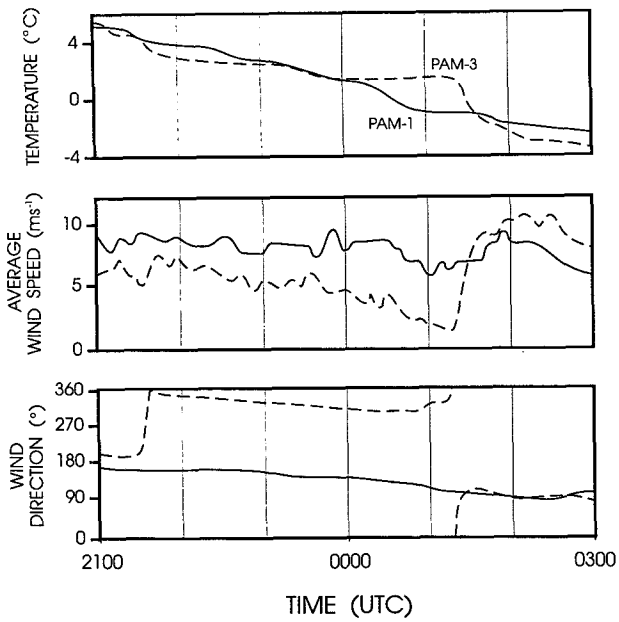

FIG. 6. Time series of temperature, 5-min average wind speed, and wind direction from PAM-1 and PAM-3. Data are from 2100 UTC 27 February to 0300 UTC 28 February.

for at least 2 h. The passage of the secondary cold front at PAM-1, on the east side of the cyclone axis, is difficult to discern since no strong frontal signatures were recorded. The slight temperature fall around 0030 was not caused by frontal passage as the front had yet to pass through Byers (BYE), the nearest station to the north (see Fig. 3c). Sublimation of virga indicated by spotty low reflectivity from MHR near PAM-1 (not shown) may have caused the observed cooling. A brief, unimpressive peak wind gust of 10 m s^{-1} at 0155, accompanied by the cessation of the backing of the winds and a slight drop in temperature marked the passage of the front there.

It is remarkable that frontal passage at these two stations was so different when they were located only 26 km apart. There were no significant differences between the two stations during passage of the initial cold front on 26 February. Thus, local effects due to topography, aside from those producing the Denver cyclone, are not likely to have caused these differences. Modeling studies by Hartjenstein and Egger (1990) demonstrated results similar to the observations described here. In their study, simulated cold fronts were allowed to interact with opposing and nonopposing flow. In the case of nonopposing flow, the cold fronts maintained their sharp leading edge and steep vertical structure; they were weaker and "flatter" when interacting with opposing flow. This may help to explain the differences between the surface measurements during the passage of the secondary front in this case.

The secondary cold front reached Loveland at 2140. By 0000 28 February the top of that frontal surface at Loveland was 600 m above ground (Fig. 4b). The secondary front lifted the boundary layer air to its lifting convection level (LCL) of 2.5 km, forming patchy cloud from 2.5 to 2.8 km. The Denver ceilometer recorded cloud bases at about 2.4–2.7 km from 1900 until 0200 (Fig. 7). The saturated, old frontal inversion air was also lifted to between 2.8 and 3.5 km. The additional lift of this layer, beyond that due to the

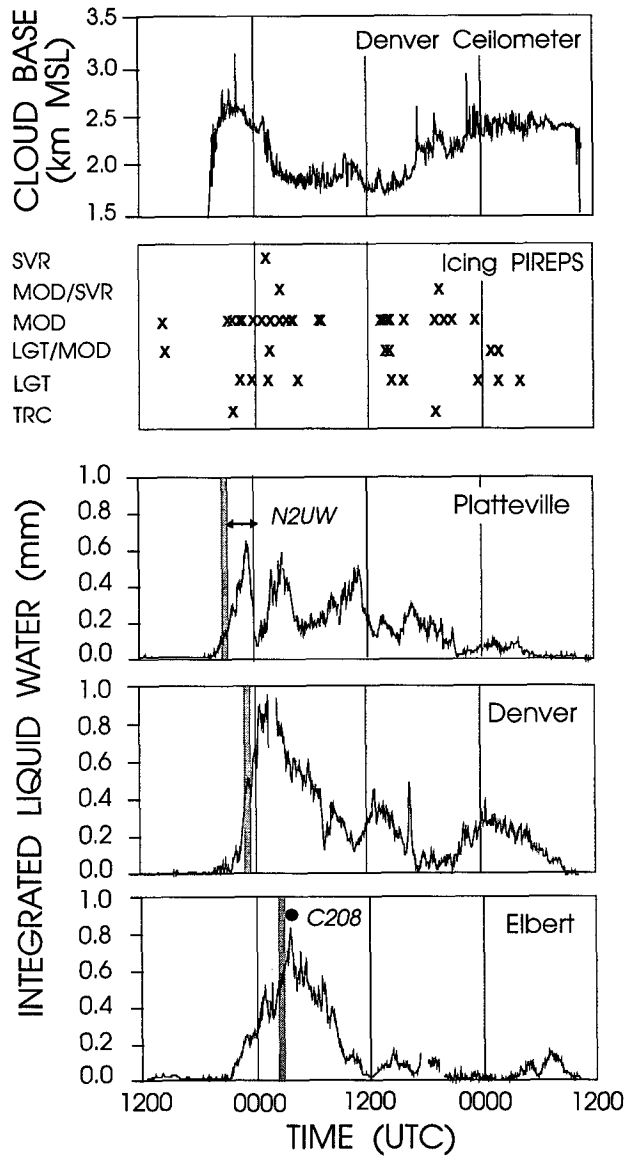

FIG. 7. Conditions between 1200 UTC 27 February and 1200 UTC 1 March 1990. Integrated liquid water from ground-based microwave radiometers at Platteville, Denver, and Elbert are shown along with ceiling height from the Denver ceilometer. Pilot reports of icing within about 50 n mi of Denver are indicated by severity (TRC—trace, LGT—light, MOD—moderate, SVR—severe). Times of the *N2UW* flight and the Cessna 208 accident are indicated. Secondary frontal passages at the radiometer sites are indicated by gray-shaded vertical bars.

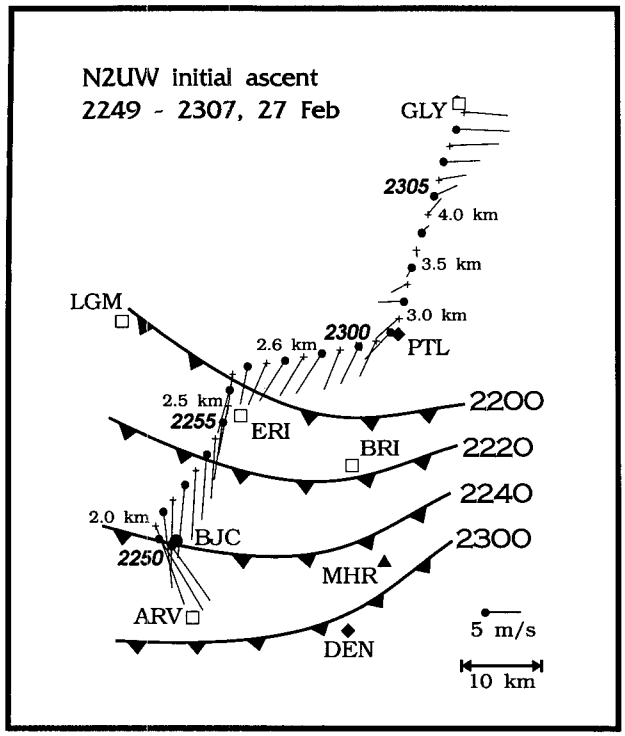

FIG. 8. The *N2UW* flight track for initial ascent from BJC. Wind flags are plotted every 30 s; scale is in the lower right corner. Locations of mesonet, radiometer, MHR, and NWS SAO sites are marked with squares, diamonds, triangles, and circles, respectively. Secondary cold front location is plotted every 20 min as barbed solid lines. Times and flight levels are indicated.

gradual deepening of the boundary layer throughout the afternoon of the 27 February, created a solid stratiform cloud with high liquid water contents.

Integrated liquid water rose rapidly at Platteville and Denver with the passage of the secondary cold front, whereas the frontal passage at Elbert was over 2–3 h later, and liquid there increased more gradually (Fig. 7). Some upslope cloud had formed over Elbert prior to passage of the secondary front, with integrated liquid near 0.4 mm. At Platteville, integrated liquid increased from near 0 to greater than 0.6 mm between 2030 and 2330, while values at Denver exceeded 0.9 mm by 0330. CLASS soundings in the WISP domain for these time periods indicate that all clouds above the stations were supercooled. Numerous pilot reports of moderate to severe icing were recorded in the area, as shown in Fig. 7.

4. Cloud structure

a. Production of supercooled liquid water

At 2249, *N2UW* took off from Jefferson County Airport (BJC in Fig. 1) and flew to the northeast during its initial climb to 4.6 km. Takeoff was approximately the time of the secondary cold frontal passage at BJC. The flight path for the ascent is shown in Fig. 8, along with surface cold front positions every 20 min and aircraft-measured winds every 30 s. The *N2UW* soundings of temperature, dewpoint, θ, and θ_e are shown in Fig. 9. The aircraft was above the secondary cold front throughout the sounding. To 2.5 km, the aircraft was within the well-mixed boundary layer, with nearly constant, θ and θ_e, with northwesterly winds near the surface, turning slightly more northerly with height. Scattered clouds were encountered from 2.5 to 2.8 km. Solid cloud was present between 2.8 and 3.3 km, within the air remaining from the initial cold front. A shallow inversion of less than 1°C marked the boundary between the two cloud layers. The top of the solid cloud was at the top of the initial cold-frontal surface, with a temperature inversion of about 4°C, rapidly increasing θ and θ_e, and a change in wind direction to westerly.

Measurements of microphysical parameters from *N2UW* obtained during the initial ascent through cloud are shown in Fig. 10. At this time, the solid portion of the cloud was 645 m thick. Liquid water contents reached 0.5 g m^{-3} near the top of this cloud. Mean droplet diameters, not shown in the diagram, were 10–13 μm. Low concentrations of precipitation particles, measured with the 2D-P probe, were present throughout the sounding. The low concentrations are consistent with the relatively warm temperatures in the cloud. However, some 2D-P images were also observed above this cloud, which could have originated from another cloud, well above the flight level, which produced light ice crystal showers. The images within the cloud were of heavily rimed particles and graupel. Above, plates and dendrites were observed.

b. Depletion of supercooled liquid water—Overview

At 2200, an infrared satellite image (not shown) indicated scattered clouds with cloud-top temperatures between −16° and −30°C over Platteville. No precipitation was associated with these clouds. Additional cold clouds were present over southeastern Colorado, the central Colorado Rockies, and southeastern Wyoming, producing light snow showers. Convective

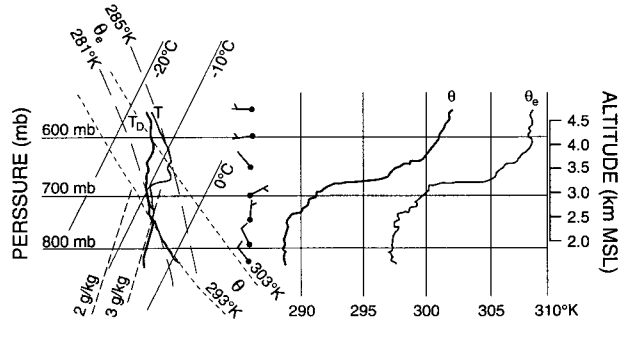

FIG. 9. Temperature and dewpoint (°C), θ and θ_e (K) from initial *N2UW* ascent northeast of BJC.

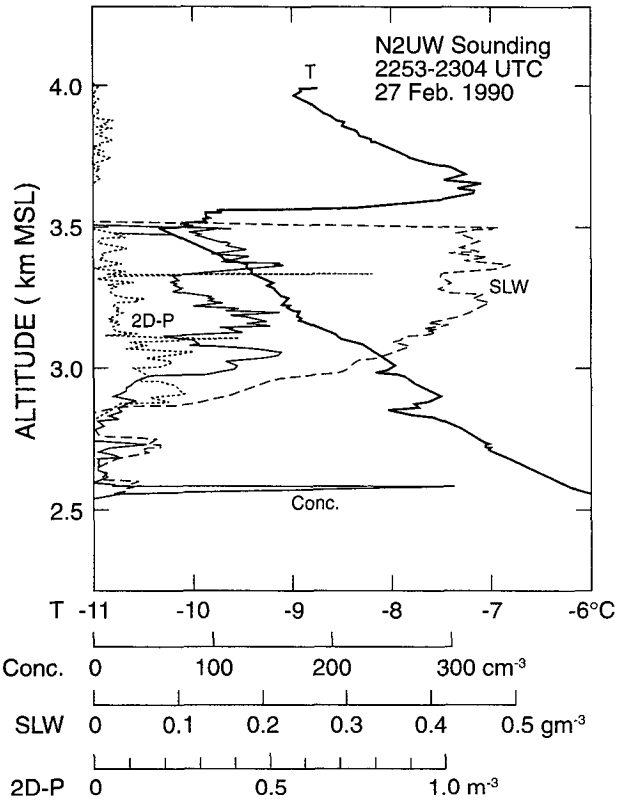

FIG. 10. Measurements of cloud droplet concentration (Conc., thin solid line), supercooled liquid water content (SLW, long dashed line), temperature (T, thick solid line), and precipitation particle concentration (2D-P, short dashed line) obtained from *N2UW* during the initial ascent from BJC. Droplet concentration is from the FSSP, liquid water content is from the King probe, and precipitation particle concentration is from the 2D-P probe.

cloudiness over the mountains was likely related to the approach of the weak short wave from the southwest. During the day thunder was recorded in NWS SAOs from southwest Colorado. By 2230, the colder cloud tops over Platteville had dissipated and/or moved to the northeast, leaving cloud-top temperatures of −10° to −16°C (see Fig. 11a). At this time, no reflectivity of greater than 5 dBZ was recorded by either the Mile High or CP-3 radars in the vicinity of Platteville and Denver. The reflectivity fields shown in Figs. 11b,d, and f are contoured values of the maximum reflectivity recorded by both the Mile High and CP-3 radars across a Cartesian grid at 3.2 km MSL. By 2300, colder cloud tops moved off the foothills to just southwest of Platteville. It appears that ice crystals fell from the upper cloud layer through the "clear" air in between, moistening and cooling the air over Platteville, as was the case with the orographically induced cloud over Loveland between 1730 and 1900. Eventually, the air moistened enough so that crystals survived the fall to enter the lower, primarily liquid, cloud now in place, where they became heavily rimed. Observations from volunteers at Loveland, Boulder, and central Denver (more than 10 km west of DEN on Fig. 1) indicated that very small graupel and heavily rimed stellar and dendritic crystals began to fall between 2300 and 2400. While graupel could have originated in the lower cloud, any dendrites must have come from aloft. By 2330, some of the higher clouds had reached Platteville, and reflectivity of greater than 10 dBZ formed over that site by 2346, extending to the northeast (see Figs. 11d, f). This snow shower was about 20 km in width and 60 km in length at this time.

Average reflectivity values from the CP-3 radar were calculated at 500-m vertical intervals for a 10 km × 10 km (x–y) area centered over the Platteville radiometer for comparison with integrated liquid water values recorded there (see Fig. 12). The data that were averaged were initially remapped into a Cartesian grid with spacing of 0.5 km in the vertical and 1.0 km in the horizontal, and were calculated at 10-min intervals between 2200 27 February, and 0400 28 February. Data from the surface (~1.4 km) to 2.8 km were eliminated due to contamination by ground clutter from the Platteville Ridge (see Fig. 1 for location). Since the upper cloud-base height was between 4.2 and 4.7 km and the top of the lower cloud was about 3.5 km, Fig. 12b depicts the reflectivity from just below the top of the lower cloud to the upper cloud layer.

Integrated liquid water measured at Platteville reached a peak of 0.67 mm at 2339, approximately 2 h after secondary frontal passage. At that time, a rapid increase in radar reflectivity over the radiometer occurred as the upper-level snow shower moved over Platteville. Reflectivities rose from below 0 dBZ throughout the column at 2305 to values greater than 12 dBZ between 2342 and 0001, while integrated liquid water decreased to 0.09 mm by 0033. One way to characterize this decline is by an exponential depletion as described by $\mathrm{ILW} = \mathrm{ILW}_0 e^{-t/\tau}$, where ILW_0 is an initial value and τ is a characteristic decay time for the liquid. These coefficients were determined by applying a least squares best fit to the radiometer-measured ILW, and provided ILW_0 of 0.73 and τ of 28 min.

As the snow shower moved to the southeast, reflectivity in the column gradually decreased, and integrated liquid water gradually recovered to predepletion values. This recovery could have been within the cloud formed by lifting of the moist layer, or new liquid created within the cold postfrontal air. The 0300 Loveland sounding (not shown) placed the cold-air depth at nearly 1 km, with an LCL of 1.7 km. Near this time, the cloud base measured by the Denver ceilometer dropped to 1.7–1.8 km (Fig. 7), consistent with this LCL.

A similar time–height cross section created for the Denver radiometer site (not shown) suggests little or no seeding from cold clouds aloft; reflectivity never exceeded 2 dBZ in the column and integrated liquid water content, which exceeded 0.9 mm, did not exhibit the sudden decrease recorded at Platteville. Instead, a

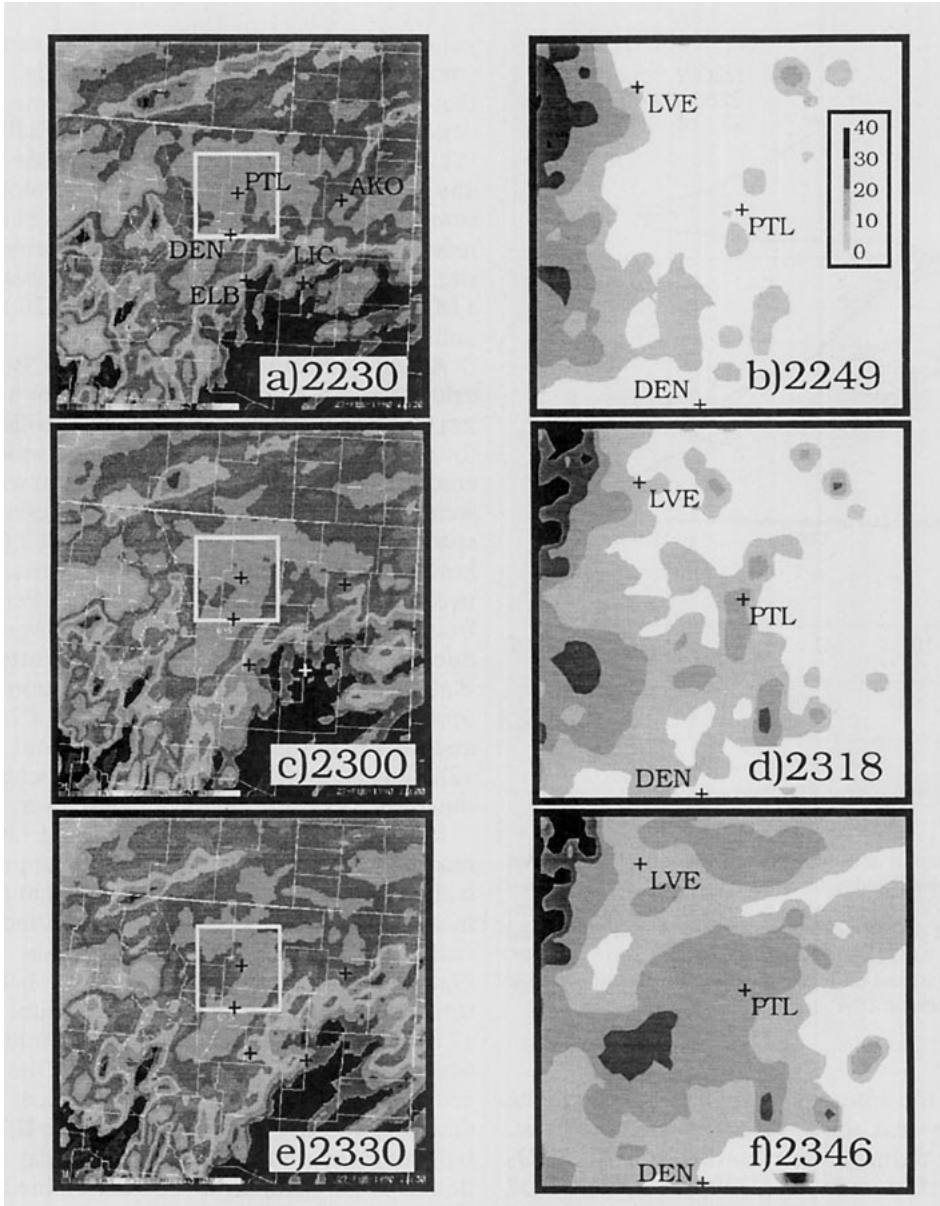

FIG. 11. Infrared satellite imagery for (a) 2230, (c) 2300, and (e) 2330 UTC 27 February 1990. Light gray areas have cloud-top temperatures between −10° and −16°C, while the darker areas are temperatures below −16°C. Constant-altitude planned position indicator (PPI) plots of combined CP-3 and Mile High Radar reflectivity at 3.2 km MSL for (b) 2249, (d) 2318, and (f) 2346 UTC are also shown; scale is indicated. Some ground clutter exists just west of LVE. Locations of PLT, DEN, ELB, LVE, AKO (Akron), and LIC (Limon) are indicated by crosses. Area of the radar plots is indicated by a white box on each satellite image.

steady increase was seen until 0100, when values began a slow decline. This could represent gradual dissipation of the cloud formed above the frontal surface, until replaced by cloud in the cold air itself. Conditions at Elbert were similar with no significant depletion due to seeding from an upper-level cloud. The integrated liquid at Elbert never reached the values achieved at either Denver or Platteville, as shown in Fig. 7. It may be that the cold air at that site, which is near the top of the Palmer Divide, never became deep enough to form its own cloud.

Rauber et al. (1986) documented several cases of liquid depletion, with timescales on the order of an hour or less, for orographic wintertime clouds in northern Colorado. Liquid was depleted as snow showers occurred. Similar studies including that of Heggli et al. (1983) documented an inverse correlation between in situ liquid water measurements and pre-

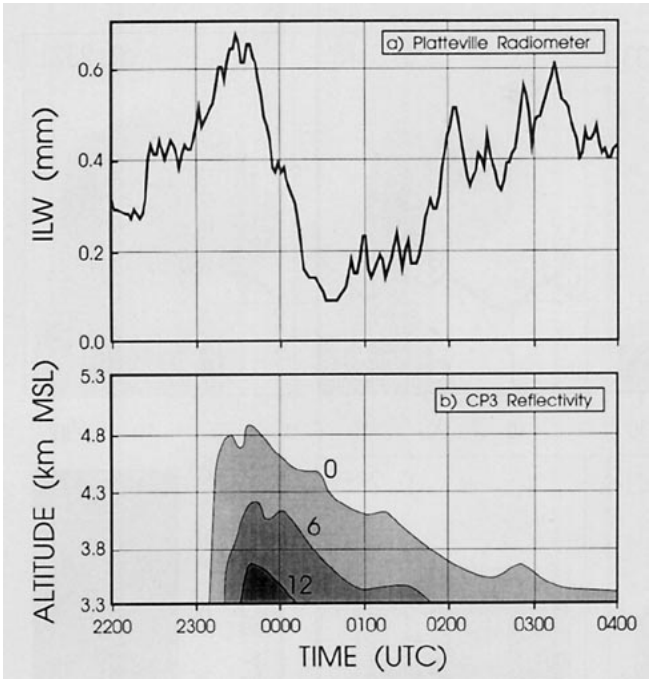

FIG. 12. Radiometer and CP-3 radar data for 27–28 February 1990 over Platteville. Top frame is integrated liquid water (ILW); lower frame is a time–height cross section of radar reflectivity, with contours labeled in dBZ.

cipitation rate in winter storms; the aircraft measurements of the lower liquid cloud and its interaction with the snow showers from aloft will be described in the next two sections.

c. *Depletion of liquid: Details of aircraft and radar data*

After the initial sounding north of BJC, *N2UW* flew a series of flight legs oriented south-southwest to north-northeast near Platteville. The CP-3 radar performed range–height indicator (RHI) scans over the Platteville area every 9 min during this time. These data were rotated into a vertical plane that roughly followed the *N2UW* flight tracks (at 29.15° from true north, see Fig. 1), then interpolated to a Cartesian grid with its origin at the southwest extent of the *N2UW* flight track. All distances described here are relative to that origin. A set of vertical cross sections of the radar reflectivity field were then created for altitudes of 2.0–6.0 km during the period of flight. Ground clutter from the Platteville Ridge was removed from the analyses by blocking out the grid points affected by it during a clear-air situation (lower left corner of Figs. 13 a–g).

At 2253, Fig. 13a shows a region of reflectivity between −5 and 10 dBZ was present below 3.0 km, extending from 13 to 35 km (distance north-northeast along the flight path). This feature corresponds to light freezing drizzle and snow grains originating from the low-level cloud. Also, a small patch of −5- to 5-dBZ reflectivity existed above 4 km and between 20 and 30 km. This feature will be referred to as cell A, and was formed within the westerly flow above the boundary layer. Cell B was located slightly south–southwest of cell A, between 11 and 18 km, and first appeared at 2303 (Fig. 13b). Between 2301 and 2306, *N2UW* passed beneath cell B as well as through the lower part of cell A and recorded 1–2 L^{-1} of graupel. Dendrites and plates were also observed in low concentrations (a few tenths per liter) beneath cell B.

By 2313, cell A descended slightly and cell B intensified to more than 0 dBZ. Again *N2UW* flew through the lower portion of cell A at 2311 and dipped into the lower liquid water cloud briefly between 2310 and 2315 (see Fig. 13c). Concentrations of ice crystals near the base of cell A approached 6 L^{-1}, with dendrites and indeterminate particles (too small and/or oddly shaped to accurately determine habit) predominating. By 2321 (Fig. 13d), cell A had descended to the lower cloud and its reflectivity rapidly increased to greater than 10 dBZ, as ice crystals grew by riming. Cell B had also begun to descend but had not yet reached the lower cloud. The liquid cloud at the base of cell A was sampled by *N2UW* and ice crystal concentrations of up to 30 L^{-1} were found, mostly dendrites and sector plates, some with light rime apparent.

At 2324–2326, *N2UW* flew above the lower cloud at 3.5 km until just beyond cell A, then climbed to 3.8 km to obtain additional measurements in the ice crystal showers. Between the cloud layers, visibility was unobstructed by the snow showers; videotapes and still camera photos from the *N2UW* clearly show features of both cloud decks. The upper deck near the northern ends of the flight legs, which was present in elongated patches, appeared solid and bubbly, suggesting convective elements, while the lower cloud layer had mostly smooth tops with some rolling, bumpy features. The presence of lightly rimed crystals between the two cloud layers implies that some liquid water was present in the upper-level cloud. The temperature range of the upper cloud would have been approximately −16° to −20°C. Further south, toward Denver and Elbert, only wispy clouds were seen aloft.

From 2322 to 2329, low concentrations of graupel (1–2 L^{-1}) were observed in the upper portion of cell A, above the lower cloud (see Figs. 13d,e). Many of the particles were small and of indeterminate type. Total concentrations were as high as 25 L^{-1}. Figure 14 shows 2D-C and 2D-P probe size ranges of 0.2–2 and 0.6–5 mm, respectively. The cell boundaries shown on this figure are approximations based both on the flight track/radar RHI comparisons in Fig. 13 and the aircraft particle data. At approximately 10–20 km (2325–2327), the aircraft was likely passing through the core of cell B as the cell descended between the 2321 and 2331 radar scans shown in Figs. 13d,e. Graupel and rimed dendrites were both present sporadically in concentrations to 2 L^{-1}. The highest ice particle concen-

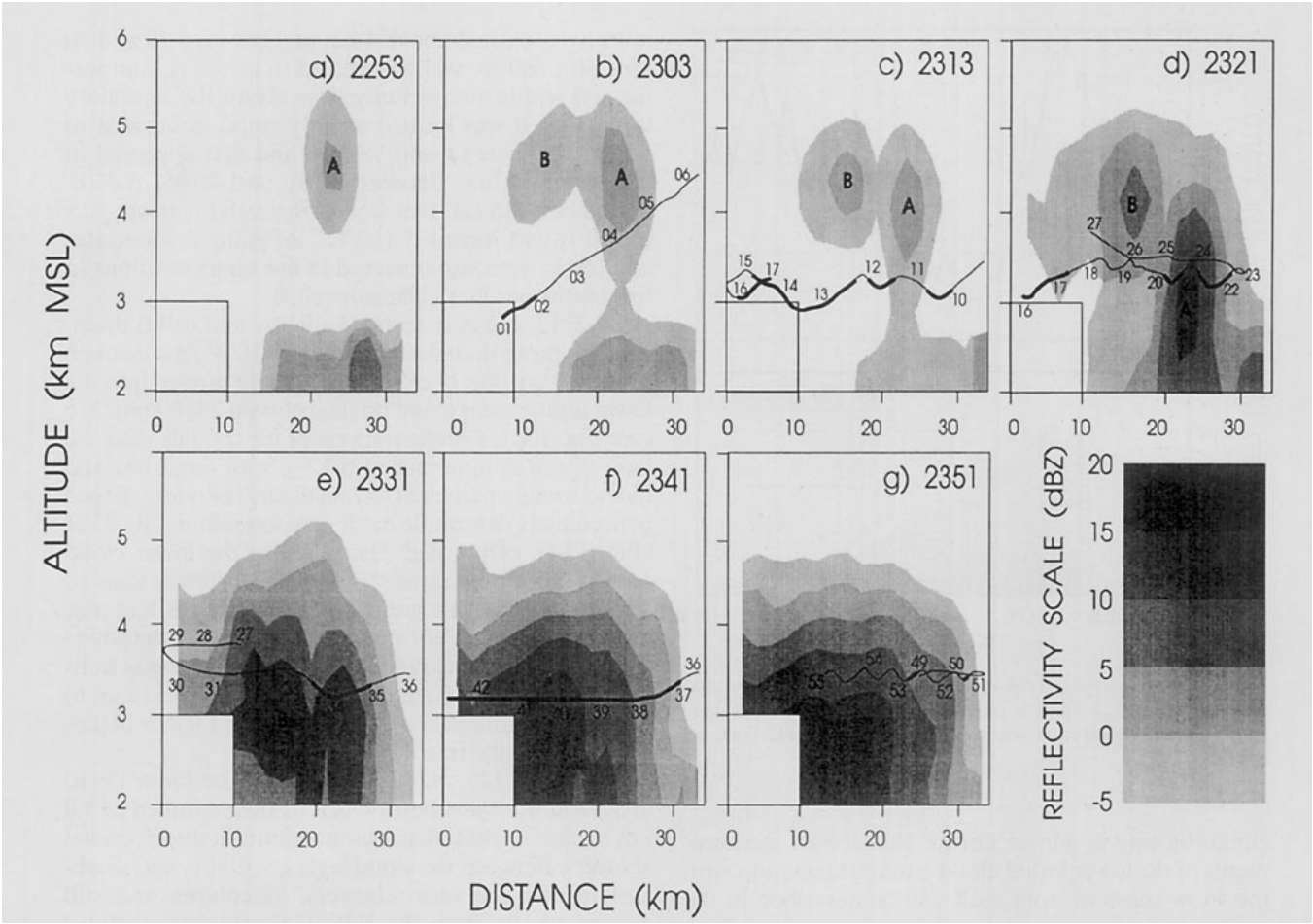

FIG. 13. Cross sections of radar reflectivity from 2253 to 2351 UTC 27 February 1990. Construction of these diagrams is described in the text. The flight track from *N2UW* projected onto the plane of the cross section is shown. Thickened areas of the flight track indicate where the aircraft sampled liquid of greater than 0.1 g m^{-3}. A reflectivity scale is at the bottom right. The heights of the base and top of the lower cloud are about 2.5–2.8 and 3.3–3.5 km, respectively.

trations and sizes were in cell B near 12 and 20 km. The region near 12 km was narrow and can be tracked through the next two cloud passes. The aircraft data resolve this feature well, whereas the radar analysis tends to blend it with the other echoes in that area, probably due to the smoothing applied to the data.

The aircraft descended to 3.5 km for another pass just above the top of the lower cloud between 2330 and 2336. By this time both cells A and B had descended into the lower cloud, and reflectivity greater than 0 dB*Z* became more widespread as showers from the upper cloud continued to develop and expand (see Fig. 13e). Ice particle concentrations in cell B were slightly lower than observed several minutes earlier at altitudes just 200–300 m higher; most of the cell was by this time below the aircraft's altitude. The larger particles were graupel and rimed dendrites.

Between 2337 and 2343, the aircraft descended into the lower cloud and flew at a constant altitude, near 3.2 km, through the remains of cells A and B (see Fig. 13f). The two cells were merging and becoming less distinct by 2341. Reflectivity increased along the entire cross section and was greater than 15 dB*Z* throughout much of the area below 3.5 km and between 10 and 25 km. As the aircraft descended into cloud, 1D-C particle concentrations were relatively high at 200–400 L^{-1}. Droplet, zero-area, and splash images were recorded by the 2D-C, which strongly suggests that large ($> \sim$30–50 μm) liquid water droplets were present. Splash images tend to occur during sampling of regions with high liquid water contents and relatively warm temperatures, a situation that does not allow for the release of latent heat quickly enough to allow the impacting water droplets to freeze onto the protruding probe arms. As the aircraft proceeded to the southwest, through the remnants of cell A, 2D-C graupel concentration and total particle concentration from the 2D-P (most images were too small to determine particle type) reached their maximum values. Cell B had also merged with the lower cloud but was still recognizable from aircraft measurements at 2341. A peak in 2D-P particle concentration lay between 10 and 15 km, cor-

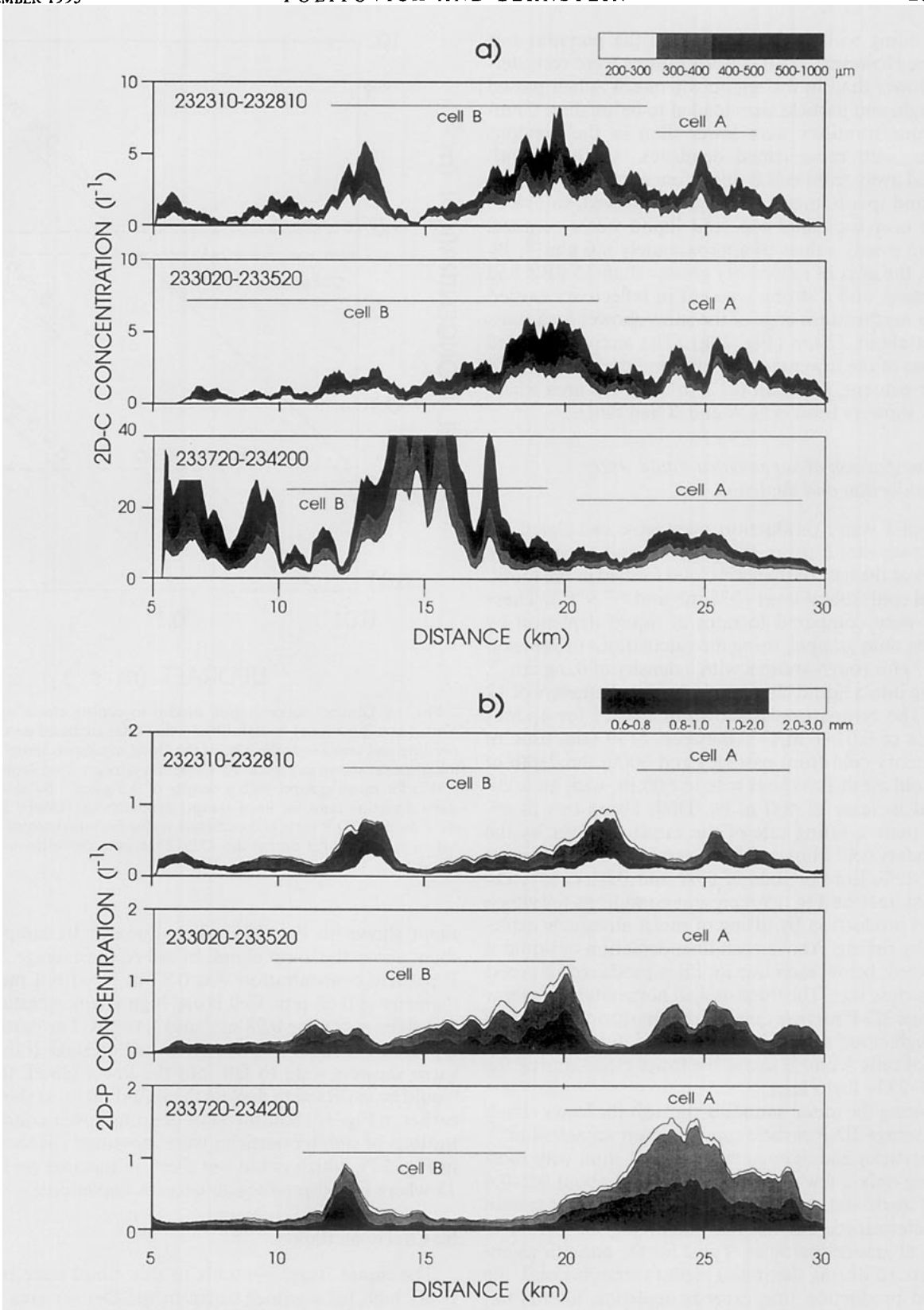

FIG. 14. Concentrations of hydrometeors measured by the (a) 2D-C and (b) 2D-P probes onboard *N2UW* for the three passes shown in Figs. 13d–f. Approximate distances corresponding to those in Fig. 13 are indicated. Shadings for different size categories are noted on the diagrams.

responding with peaks observed in the previous two passes. However, 2D-P concentrations were considerably lower than in the region where cell A had passed through, and particle sizes tended to be smaller. Graupel concentrations were lower than in the previous passes, with more rimed dendrites. As the aircraft moved away from cell B, high concentrations of zero-area and splash images were again observed, similar to those near the cloud top, and liquid water contents rose to steady values of approximately 0.6 g m^{-3}. By 2351, the area of reflectivity greater than 15 dBZ had increased, and a strong gradient in reflectivity existed at the northeastern edge of the snow shower area starting at about 22 km (Fig. 13g). The aircraft sampled the top of the lower cloud and found decreased liquid water content, less than 0.1 g m^{-3}, in the area where snow showers from cells A and B had fallen.

d. Comparison of supercooled liquid water production and depletion

Liquid water production rates were calculated for the lower cloud using the pressure and temperature values at the base of the solid cloud formed in the moist, initial cold frontal layer (736 mb and −7.9°C). These rates were compared to rates of liquid depletion by riming onto graupel, using the calculations of Johnson (1987) for rough graupel with a density of 0.3 g cm^{-3}, falling into a liquid cloud with droplet diameters of 12 μm. The comparison is shown in Fig. 15 for updraft speeds of 0.01–1 m s^{-1}. Between 2130 (the time of secondary cold front passage) and 0000, the depth of the cold air at Loveland rose to 600 m, with an additional increase of 400 m by 0300. Using this to approximate a lifting rate of the moist air layer by the secondary cold front provides average updraft estimates over these time periods of 0.07 and 0.04 m s^{-1}. Diagonal lines on Fig. 15 represent conditions for which liquid production by lifting of moist air equals depletion by riming. Above each line, depletion of liquid is expected; below each line liquid is produced in excess of the rime rate. The three dashed horizontal lines show average 2D-P particle concentrations during the ascent through cloud shown in Fig. 10, and during interception of cells A and B above the lower cloud during the 2329–2336 flight leg.

During the initial sounding through the lower cloud, the average 2D-P particle concentration was 0.054 m^{-3}. All particles had diameters less than 1 mm, with most having only a few pixels (equivalent to about 0.2–0.6 mm) shadowed. At these sizes, 2D-P image type cannot be determined, but the accompanying 2D-C images were of graupel particles. Thus, for the conditions encountered during the initial ascent through cloud, the liquid production rate exceeds depletion for updraft speeds in the ranges expected.

Higher 2D-P particle concentrations and diameters were measured in cells A and B during the flight segment shown in Fig. 13e, when the aircraft sampled them above the lower cloud. In cell A, the average 2D-P particle concentration was 0.87 m^{-3}, with a mean diameter of 0.68 mm. Cell B had higher concentrations and sizes, averaging 0.98 m^{-3} and 1.1 mm. The particle types were graupel and heavily rimed crystals. If these snow showers were to fall into the lower cloud, they would be expected to deplete the liquid there, as shown earlier in Fig. 12. Southwest of the cells, lower concentrations of smaller particles were measured (as shown in Fig. 14), which could put them in the area on Fig. 15 where liquid production exceeds depletion.

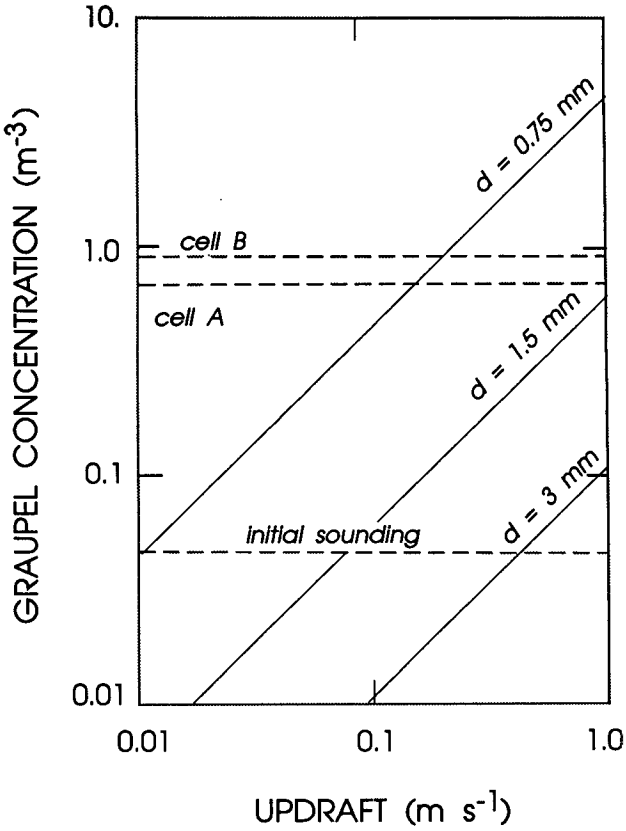

FIG. 15. Graupel concentration needed to deplete cloud liquid plotted as a function of updraft. Production rates are based on temperature and pressure at the base of the cloud measured during the initial ascent shown in Figs. 8–10. Depletion rates are from Johnson (1987) for rough graupel with a density of 0.3 g cm^{-3}. Solid lines show depletion rates for three graupel diameters (d). Dotted lines show average 2D-P particle concentrations for the initial ascent and within cells A and B during the 2329–2336 pass above the liquid cloud.

5. Effects on flight

The liquid water contents in this cloud were relatively high for a winter storm in the Denver area (as in Reinking and Boatman 1986), and, as mentioned previously, led to many reports of moderate and severe icing in the area. Measurements from *N2UW* allow

quantification of the icing hazard. Porpoising maneuvers were conducted throughout the flight to obtain a wide range of angle of attack for precise calculation of the coefficients of lift (C_L) and drag (C_D) on the airframe. These values were derived using the methods discussed in Sand et al. (1984) and are listed in Table 1, along with the clean aircraft values.

During the initial sounding through cloud, substantial ice accumulated on the airframe. The coefficient of drag C_D increased by 38%. Coefficient of lift was essentially unchanged; the calculated value is within the 5% uncertainty reported by Cooper et al. (1984) for the derivation. After two more passes through the lower cloud, the pilot climbed above cloud and noted that the maximum rate of climb (ROC) possible was around 2.5 m s^{-1} (normally the aircraft has about 7–10 m s^{-1} climb capability). Performance calculations for the time period 2323–2333, when the aircraft was in snow showers between cloud layers, showed a 58% increase in C_D and a slight reduction in C_L.

During the 2336–2342 pass, the highest liquid water contents during the flight were encountered as the aircraft flew toward the southwest, away from snow showers falling from an upper cloud, which depleted liquid water as described in the previous section. Mean droplet diameters near the top of the lower cloud during this pass, shown in Fig. 16, were 20–25 μm. In this portion of the cloud, 1D-C concentrations were highest, to over 200 L^{-1}. Images from 2D-C indicate low concentrations of ice were present in the cloud, but high numbers of splash images suggest that the majority of 1D-C-measured particles are likely to have been water droplets. During the time of level flight, after about 2338, the mean diameter remained fairly constant at 17–22 μm, FSSP-measured droplet concentration rose, and 1D-C concentration decreased. Thus, the higher liquid amount was contained in smaller droplet sizes—the contribution to icing from the 1D-C was small. At approximately 2343, the pilot decided to climb above cloud to sublimate the accumulated ice, since the aircraft's performance had declined substantially. At 2347, above the lower cloud, a stall check produced a pronounced buffet at an indicated airspeed of 115 kt (59 m s^{-1}); the normal stall speed of this aircraft is about 90 kt (46 m s^{-1}). Between 2347 and 2352 the aircraft performed a final set of maneuvers for lift and drag coefficient determination. The values listed in Table 1 indicate effects on lift and drag similar to those from the previous two calculations: small lift decrease but greatly increased drag. After this final pass through the cloud, C_D increased by 84% over the clean aircraft values.

Size distributions from this cloud pass, from near the cloud top and during level flight, are shown in Fig. 17. In both distributions, there is a peak at 10–18 μm, with a sharp decrease at larger FSSP-measured sizes. The 1D-C portions of the spectra lie several orders of magnitude below the small droplet peak in both cases,

TABLE 1. Coefficients of lift (C_L) and drag (C_D) for *N2UW* calculated during specified times on 27 February 1990.

Time (UTC)	C_L	C_D	Percentage increase in C_D
Clean aircraft	0.590	0.036	—
2303:10–2304:10	0.636	0.050	38
2323:00–2333:00	0.531	0.057	58
2350:40–2356:10	0.602	0.068	84

but concentrations of large droplets (> ~50-μm diameter) were higher nearer the top of the lower cloud (dashed line in Fig. 17a). Total droplet concentration (FSSP and 1D-C combined) from 2337:30 to 2338:00 was 14.7 cm^{-3}; from 2342:00 to 2343:00 it was 121.9 cm^{-3}. It is possible that, especially for the latter flight segment, measurements of droplet concentration from both probes were lowered due to restricted sample areas caused by icing. The effect this would have on droplet sizing is unknown.

Differences in the droplet size distributions in the large droplet range are greatly emphasized when considering the mass contributions to ice accumulation. An estimate of the mass contribution as a function of droplet size is shown in Fig. 17b. The mass of liquid from each size bin of the FSSP and 1D-C was first derived, then adjusted by the collection efficiency of the mean size of the bin. The collection efficiency used was that for a 3-in.-diameter cylinder traveling perpendicular to the airstream at the measured airspeed of *N2UW*. This collector is considered a standard in ice-accretion calculations, such as those described by Lewis (1951). The resulting peaks in mass contribution reside in the FSSP size range for both distributions. However, nearer the cloud top, the contribution from large droplets was considerably greater than lower in the cloud. Icing caused by larger droplets can have a greater effect on flight than that resulting from smaller (diameters less than approximately 30 μm), as described by Sand et al. (1984) and later by Politovich (1989).

Figure 18 shows photographs, taken after landing, of ice on several probes and on one of the propeller spinners. Just after 2343, the 2D-C probe, which is the probe farthest back in Fig. 18a, totally iced over so that no data were available for most of the remainder of the flight. The photo shows a block of ice aft of the leading end of the top probe tip. Ice accretions on the FSSP, which is the probe in the foreground, are limited to the leading ends of the probe tips. These tips are heated; in the case of the 2D-C, the heat may have melted a hole in the ice and allowed it to slip back and obscure the aperture. Until the 2337–2343 pass through the lower cloud, ice on the propeller spinners was confined to a narrow plug near their centers. Following the pass, ice was observed over larger areas and several inches aft of the forwardmost points, as shown in Fig.

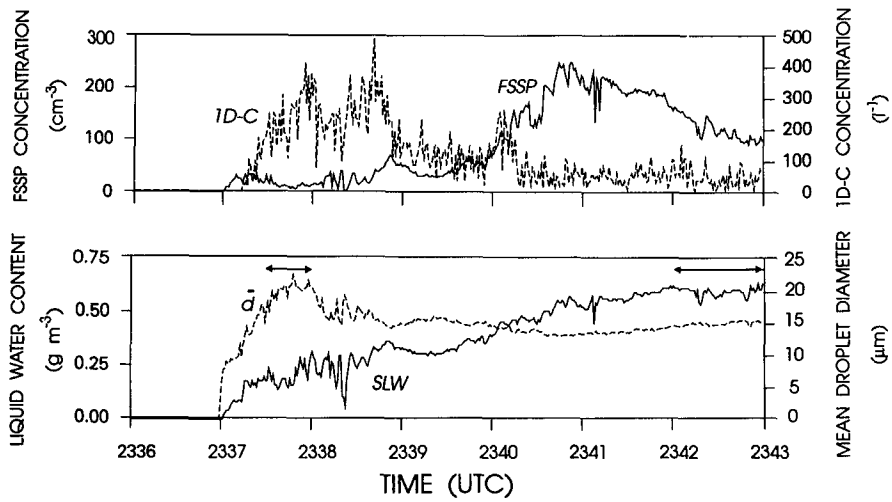

FIG. 16. Droplet concentration (FSSP), mean droplet diameter ($\bar{d}$), supercooled liquid water content (SLW), and 1D-C hydrometeor concentration (1D-C) from *N2UW* for 2336:00–2343:00 UTC 27 February 1990. Horizontal arrows indicate times of size distributions shown in Fig. 17. Time-to-distance scaling is approximately 1 min to 6 km.

18b. As a droplet's diameter increases, so does its momentum, which allows crossing of flow streamlines and impaction farther away from the forward stagnation point. Thus, the location of ice accretion on portions of the aircraft could be used as an (uncalibrated) indication of relatively large droplet diameters. Underwing icing was observed with a video camera mounted to allow inspection of that area, and the flight technician noted that ice had accreted on side windows near the rear of the aircraft, something he had not seen before.

Since the pilot found it necessary to divert from the area of icing, the conditions were, by definitions of severity used in reporting icing, in the severe category. Lewis (1951) proposed an index system to define these reporting definitions, based on liquid water content, droplet size, and temperature. Under this system, the intensity of icing encountered during the 2336–2343 pass would have been moderate at most. Further adjustments to those category definitions may be needed to more appropriately reflect the effect of meteorology on flight.

6. Summary

On 26 February 1990, a shallow cold front passed through northeastern Colorado. This front, and the broad high pressure area behind it, set up a Denver

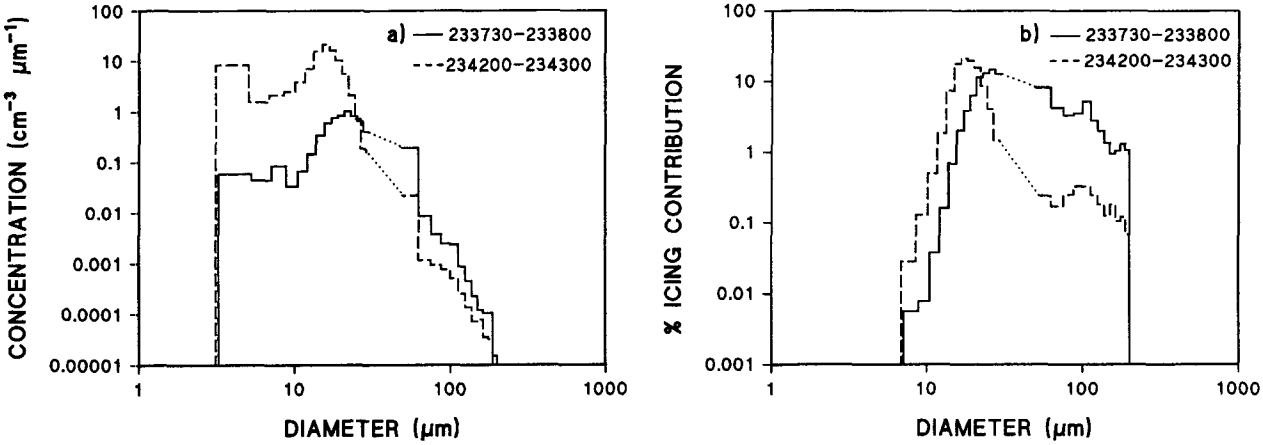

FIG. 17. FSSP and 1D-C data from *N2UW* for 2337:30–2338:00 and 2342:00–2343:00 UTC 27 February 1990: (a) droplet size distribution, (b) percentage mass contribution to icing. Calculation of (b) is described in the text. The dotted line bridges the gap between the FSSP and the 1D-C size ranges.

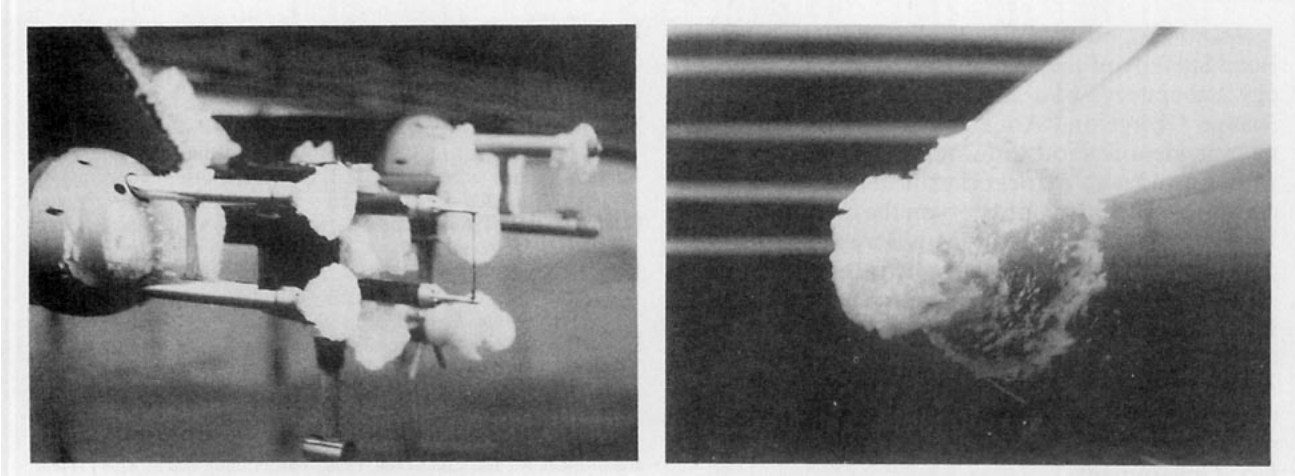

FIG. 18. Photographs of icing on *N2UW* obtained after the 27 February 1990 flight (a) on the FSSP, King probe, Johnson–Williams, reverse-flow temperature, and 2D-C probes and (b) on the starboard propeller spinner.

cyclone circulation that was well in place by the afternoon of 27 February. Later that afternoon, a secondary cold front passed through the WISP domain, which interacted with the existing atmospheric structure. The well-mixed boundary layer containing the circulation was lifted to form scattered cloud, while a nearly saturated layer above that, representing the remains of the original cold front, formed a stratiform cloud containing high liquid water contents and hazardous icing conditions. Integrated liquid water values were highest in the 3–6 h following the passage of the secondary front, as the initial lifting of the prefrontal air generated high amounts of liquid in a relatively warm cloud. Subsequent upslope flow behind the secondary cold front produced long-lived but colder cloud, with lower integrated liquid water contents, for over 36 h.

Depletion of liquid took place in limited areas as ice crystals were produced in midlevel clouds embedded in westerly flow. Snow showers formed that were oriented southwest to northeast on scales of about 20 km in width and up to 60 km in length. Ice crystals fell about 1 km through cloud-free, but moist, air into the lower cloud layer and depleted integrated liquid water to as little as one-sixth of its predepletion value within 1 h. Aircraft observations show that these crystals were lightly rimed as they fell from the upper-level cloud and became heavily rimed, turning to graupel, as they fell through the lower cloud. Precipitation at the ground was light and consisted of snow grains, snow, and freezing drizzle, and was likely a mixture of precipitation formed within the lower layer itself, and that which was falling from above, depending on location. The highest radar reflectivity in the area was 15–20 dBZ. Undepleted liquid water values measured with a research aircraft exceeded 0.6 g m^{-3}, placing this icing environment in the moderate category for stratiform clouds as defined by Lewis (1951). If it is assumed that reductions in liquid water content follow the same trend as integrated liquid, icing severity should have decreased to the trace or light category. Thus, on a timescale of less than 1 h, and a spatial scale of around 20 km, the icing characteristics of the cloud were changed significantly. The icing affected *N2UW*'s flight in this case mostly by increasing drag on the airframe.

As part of WISP, methods have been developed to use output from operationally available national-scale weather forecast models to predict areas that have a potential for in-flight icing (Schultz and Politovich 1992; Thompson et al. 1995). To date, the Nested Grid, eta, and Rapid Update Cycle Models have been used. Since none of the current operational versions of these models include explicit calculations of liquid water content, the surrogate outputs of temperature and relative humidity are thresholded to provide reasonable estimations of where icing conditions are likely to reside, provided there are clouds there. Horizontal grid spacing ranged from 60 to 80 km in tests of the techniques.

The results of this study strongly suggest two areas where attention must be focused in order to provide accurate icing forecasts. First, horizontal and vertical model scales must be appropriate for simulation of the mesoscale features that lead to local enhancement and reduction of supercooled liquid, and thus the icing hazard. This is particularly relevant for icing depictions for an airport terminal area, where scales of time and space of less than 1 h and less than 100 km must be carefully considered. Also, the capability must be developed within numerical forecast models to explicitly predict the presence of supercooled liquid water. The models must be able to accurately simulate both its production and depletion. The depletion processes are dependent on various complex ice–liquid interaction processes, the details of which are not completely understood. However, as this case clearly demonstrates, significant variations in the icing environment can occur due to differences in liquid production and depletion on scales of 20–60 km.

Acknowledgments. We thank Ed Westwater and Boba Stankov of the NOAA Environmental Technology Laboratory, who supplied the radiometer data; Joanne George and Anne Jones, who wrote the 2D particle-identification software; and Tiffany Omeron, who assisted with particle classification. Rita Roberts contributed helpful comments on the manuscript. The National Aviation Weather Advisory Unit provided pilot reports used in this study. This research is sponsored by the National Science Foundation through an Interagency Agreement in response to requirements and funding by the Federal Aviation Administration's Aviation Weather Development Program. The views expressed are those of the authors and do not necessarily represent the official policy or position of the U.S. Government.

We hope that studies such as these will lead to forecasts that will prevent tragedies such as the Cessna 208 crash.

REFERENCES

Bernstein, B. C., I. Baker, D. Wesley, J. Smart, L. Wharton, and J. Wirshborn, 1992: The utility of a high resolution volunteer snow observer network. *Proc., 11th Int. Conf. on Clouds and Precipitation,* Montreal, PQ, Canada. Amer. Meteor. Soc., 991–994.

Cerni, T. A., 1982: Determination of the size and concentration of cloud drops with an FSSP. *J. Climate Appl. Meteor.,* **22,** 1346–1355.

Cober, S. G., G. A. Isaac, and J. W. Strapp, 1995: Aircraft icing measurements in east coast winter storms. *J. Appl. Meteor.,* **34,** 88–100.

Cooper, W. A., W. R. Sand, M. K. Politovich, and D. L. Veal, 1984: Effects of icing on performance of a research airplane. *J. Aircraft,* **21,** 708–715.

Crook, N. A., T. L. Clark, and M. W. Moncrieff, 1990: The Denver Cyclone. Part I: Generation in low Froude number flow. *J. Atmos. Sci.,* **47,** 2725–2742.

Hartjenstein, G., and J. Egger, 1990: Frontogenesis near steep orography. *Tellus,* **42A,** 259–269.

Heggli, M. F., L. Vardiman, R. E. Stewart, and A. Huggins, 1983: Supercooled liquid water and ice crystal distributions within Sierra Nevada winter storms. *J. Climate Appl. Meteor.,* **22,** 1875–1886.

Hill, G. R., 1992: Further comparisons of simultaneous airborne and radiometric measurements of supercooled liquid water. *J. Appl. Meteor.,* **31,** 397–401.

Hogg, D. C., F. O. Guiraud, J. B. Snider, M. T. Decker, and E. R. Westwater, 1983: A steerable dual-channel microwave radiometer for measurements of water vapor and liquid water in the troposphere. *J. Climate Appl. Meteor.,* **22,** 789–806.

Jeck, R. K., 1983: A new data base of supercooled cloud variables for altitudes up to 10,000 feet AGL and the implications for low altitude aircraft icing. U.S. Dept. of Transportation Report DOT/FAA/CT-83/21, 137 pp.

Johnson, D. B., 1987: On the relative efficiency of coalescence and riming. *J. Atmos. Sci.,* **44,** 1671–1680.

King, W. D., D. A. Parkin, and R. J. Handsworth, 1978: A hot-wire liquid water device having fully calculable response characteristics. *J. Appl. Meteor.,* **17,** 1809–1813.

Lewis, W., 1951: Meteorological aspects of aircraft icing. *Compendium of Meteorology,* T. F. Malone, Ed., Amer. Meteor. Soc., 1197–1203.

Politovich, M. K., 1989: Aircraft icing caused by large supercooled droplets. *J. Appl. Meteor.,* **28,** 856–868.

Rasmussen, R., and Coauthors, 1992: Winter Icing and Storms Project (WISP). *Bull. Amer. Meteor. Soc.,* **73,** 951–974.

Rauber, R. M., L. O. Grant, D. Feng, and J. B. Snider, 1986: The characteristics and distribution of cloud water over the mountains of northern Colorado during wintertime storms. Part I: Temporal variations. *J. Climate Appl. Meteor.,* **25,** 468–488.

Reinking, R. F., and J. F. Boatman, 1987: Upslope precipitation events. *Mesoscale Meteorology and Forecasting,* P. S. Ray, Ed., Amer. Meteor. Soc., 437–471.

Sand, W. R., W. A. Cooper, M. K. Politovich, and D. L. Veal, 1984: Icing conditions encountered by a research aircraft. *J. Climate Appl. Meteor.,* **23,** 1427–1440.

Schultz, P., and M. K. Politovich, 1992: Toward the improvement of aircraft-icing forecasts for the continental United States. *Wea. Forecasting,* **7,** 491–500.

Stankov, B. B., E. R. Westwater, J. B. Snider, and R. L. Weber, 1990: Remote sensor observations during WISP90: The use of microwave radiometers, RASS and ceilometers for detection of aircraft icing conditions. NOAA Tech. Memo. ERL WPL-187, 77 pp. [Available from Environmental Technology, 3100 Marine St., Boulder, CO 80303.]

Szoke, E. J., 1991: Eye of the Denver Cyclone. *Mon. Wea. Rev.,* **119,** 1283–1292.

Thompson, G., R. T. Bruintjes, and B. G. Brown, 1995: A comprehensive icing prediction and evaluation program. Preprints, *Sixth Conf. on Aviation Weather Systems,* Dallas, TX, Amer. Meteor. Soc., 243–248.

Westwater, E. R., 1993: Ground-based microwave remote sensing of meteorological variables. *Atmospheric Remote Sensing by Microwave Radiometry,* M. A. Janssen, Ed., John Wiley & Sons, 145–213.

Wilczak, J. M., and T. W. Christian, 1990: Case study of an orographically induced mesoscale vortex (Denver Cyclone). *Mon. Wea. Rev.,* **118,** 1082–1102.